



## EEG-based emotion recognition in an immersive virtual reality environment: From local activity to brain network features

Minchang Yu<sup>a</sup>, Shasha Xiao<sup>a</sup>, Minlei Hua<sup>b</sup>, Hui Wang<sup>b</sup>, Xi Chen<sup>a</sup>, Feng Tian<sup>b,\*</sup>, Yingjie Li<sup>c,\*</sup>

<sup>a</sup> Shanghai Institute for Advanced Communication and Data Science, School of Communication and Information Engineering, Shanghai University, Shanghai 200444, China

<sup>b</sup> Shanghai Film Academy, Shanghai University, Shanghai 200072, China

<sup>c</sup> School of Life Sciences, College of International Education, Institute of Biomedical Engineering, Shanghai University, Shanghai 200444, China



### ARTICLE INFO

**Keywords:**

Emotion recognition  
EEG dataset  
Spectral power  
Functional brain network  
PLV

### ABSTRACT

Emotion electroencephalography (EEG) datasets play a significant role in EEG-based emotion recognition research, providing a platform for comparisons of different emotion recognition methods. Most datasets used 2D images or videos as mood induction procedures (MIPs); however, considering the differences in EEG dynamics between 2D and 3D environments, experimental research based on 2D MIPs may have poor results being applied in a real 3D world. In this paper, we (1) developed a new emotion EEG dataset, virtual reality (VR) emotional EEG dataset (VREED), which used 3D VR videos as MIPs; and (2) Presented a baseline for the performance of negative/positive emotion classification in the new dataset. The best average accuracy of  $73.77\% \pm 2.01\%$  was obtained by using the combination of theta (4–8 Hz), alpha (8–13 Hz), beta (13–30 Hz), and gamma (30–49 Hz) relative power features. Additionally, we observed that occipital and frontal regions played a more critical role than other regions in emotion processing from Spearman correlation analysis and feature selection. This new VR emotion EEG dataset will be publicly available, and we encourage other researchers to evaluate their emotion classification methods on the VREED.

### 1. Introduction

Emotions play an essential role in human cognition, including social interaction, learning, perception, and to some degree, human intelligence itself [1,2]. With the development of human-computer interaction technology, people expect computers to have the ability to perceive and understand human emotions, which present promising application prospects in many fields. For example, clinically, medical doctors could monitor emotional states of patients with disorders of consciousness using a human-computer interaction (HCI) system for emotion recognition [3]; in many fields, such as computer games and distance education, identifying and feedbacking user emotion could enhance user experiences [4–7].

Studies of emotion recognition have been performed based on different types or modalities of data, such as facial expression, speech, and physiological signals such as electroencephalography (EEG), electrocardiogram (ECG), and pulse. Among these, EEG-based emotion recognition has attracted an increasing number of researchers in recent

years [8–11] because EEG could effectively reflect the electrical activity of the central nervous system and is associated with higher-level cognitive processes [12] and emotion [5,13]; moreover, EEG cannot be deliberately controlled or concealed [14]. In emotion recognition studies, emotions need to be elicited in laboratory environments using mood induction procedures (MIPs), such as images, audios, and videos [15–17]. Previous EEG-based emotion recognition studies are mainly based on some classical public emotion EEG datasets [18–21], such as MAHNOB-HCI [22], DEAP [23], and SEED [17], which use non-immersive two-dimensional (2D) videos or images as MIPs. However, the emotion and sense induced by 2D display are different from that by the three-dimensional (3D) real world; for example, the 2D display lacks the sense of presence and depth information [24–27]. Moreover, considering the known differences in EEG dynamics between 2D and 3D presentations [28–30], there may be a gap between the experimental studies based on 2D display and real-world applications [28]. It is necessary to develop 3D virtual reality (VR) MIPs, which enable researchers to simulate real-world conditions in a controlled laboratory

\* Corresponding author at: P.O. Box 98, 99 Shangda Road, Baoshan District Shanghai University, Shanghai 200444, China.

\*\* Co-corresponding author.

E-mail address: [liyj@i.shu.edu.cn](mailto:liyj@i.shu.edu.cn) (Y. Li).

environment, and are gaining popularity in studying emotion [31].

In this paper, we performed a systematic analysis of EEG-based emotion recognition in a 3D immersive VR environment. The main contributions are: (1) we developed a publicly available emotion EEG dataset using 3D VR videos as MIPs. As far as we know, it is the first public high-density (59 EEG channels) emotion EEG dataset that uses 3D VR videos as MIPs; and (2) We systematically compared the emotion recognition performance of various EEG features in the new dataset, providing a baseline performance for future studies. The remaining sections of this paper are arranged as follows. Section 2 provides a brief overview of related work on EEG-based emotion recognition. Next, materials used in this study are presented in Section 3; EEG feature extraction and feature selection methods used in our dataset are illustrated in Section 4; in Section 5, we present our emotion recognition results. Finally, the discussion and conclusion about this work are presented in Section 6 and Section 7.

## 2. Related work

### 2.1. Public emotion EEG datasets

The most commonly used emotion EEG datasets currently are MAHNOB-HCI [22], DEAP [23], and SEED [17]. (1) The MAHNOB-HCI published in 2011 is a multimodal dataset recorded in response to affective stimuli [22]. Twenty-seven subjects watched 20 emotional video clips selected from commercially produced movies in the first experiment and were required to rate their emotions induced by each video from multiple dimensions, such as dominance, arousal, and valence. In the second experiment of MAHNOB-HCI, subjects were shown video fragments or images with emotion labels and were asked to determine whether the labels were correct or not. Their experiment collected EEG recordings of 32 channels, eye gaze, facial expression, and other physiological signals. (2) The DEAP dataset published in 2011 contained EEG (32 channels) recordings and peripheral physiological signals of thirty-two subjects when watching 40 one-minute music videos. The subjects were asked to rate each video in the dimensions of valence, arousal, familiarity, and dominance [23]. (3) In 2017, the SEED dataset was released. Three sessions of EEG signals (62 channels) were collected from fifteen subjects when the subjects watched fifteen emotional video clips chosen from six famous Chinese films. The time interval between two sessions was no less than one week to study the stable emotional patterns over time [17].

It should be noted that all the above datasets used 2D videos or images as MIPs. In 2018, Marín-Morales et al. [1] published an emotion EEG dataset using four VR scenarios as MIPs. However, it is hard to get a full range of spatial detail in the brain's electrical fields at the scalp surface and an acceptable source localization accuracy [32,33] since they used a 9-channel low-density scalp EEG recorder.

### 2.2. Computational methods to estimate affective states

EEG-based emotion recognition can use various features, including time domain, frequency domain, and time-frequency domain features [34]. The spectral power, thought to reflect local brain activities, is the most commonly used feature [20,34–36]. For example, Koelstra et al. [23] extracted EEG spectral power features from the DEAP dataset and then classified these features into low/high valence, arousal, and liking used a naive Bayes classifier. Zhang et al. [36] classified four emotional states (relaxation, sadness, fear, and joy) on the DEAP dataset, using the power of theta, alpha, beta, and gamma bands as features. They obtained a classification accuracy of  $59.13\% \pm 11.00\%$  with a support vector machine (SVM) classifier, and they reported that the frontal and parietal EEG channels contained more emotion-related information. Using a discriminative graph regularized extreme learning machine (GELM) classifier and the power features, Zheng et al. [17] classified four emotions on the SEED dataset and obtained a classification

accuracy of 61.46% for a four-class classification task. In addition, previous studies have shown that the spectral power of the inter-hemispheric asymmetry plays a vital role in EEG-based emotion classification. The asymmetry features can be calculated by the spectral power subtraction or division and named differential asymmetry (DASM) and rational asymmetry (RASM), which reflect frequency and spatial characteristics of EEG signals. In [37], Li et al. used RASM features and Long Short-Term Memory (LSTM) network obtained a mean accuracy of 76.67% on the DEAP dataset for negative/positive valence classification.

Further, increasing studies performed emotion recognition using the topological properties of functional brain networks as classification features [20,38], which is in line with the following views: (1) the brain can be regarded as a large-scale distributed network of interconnected areas [30,39], and (2) “emotional state is likely to involve circuits rather than any brain region considered in isolation” [40]. For example, Lee et al. [41] classified three emotion states(negative, neutral, and positive) in their private dataset using functional connectivity features of all frequency bands. They observed that the classification accuracies varied depending on the connectivity types (correlation, coherence, and phase synchronization index (PSI)), 43% for correlation, 44% for coherence, and 52% for PSI using a Quadratic Discriminant Analysis (QDA) classifier. Chen et al. [38] classified emotion states on the DEAP dataset into low/high arousal and low/high valence using three connectivity measures evaluated by phase coherence, Pearson correlation, and mutual information, respectively. Using the mutual information features, they obtained the best accuracy of 76.17% on valence and 73.59% on arousal with an SVM classifier.

Recently, deep learning has also been applied to EEG-based emotion recognition research. Li et al. [37] extracted RASM features from the DEAP dataset and then achieved a mean accuracy of 76.67% for positive/negative valence using an LSTM network. Alhagry et al. [42] recognized emotions from the raw EEG signals of the DEAP dataset using an LSTM network and obtained average accuracies of 85.65%, 85.45%, and 87.99% for low/high arousal, low/high valence, and low/high liking classification, respectively. Wei et al. [14] extracted EEG differential entropy (DE) features of the SEED dataset. They obtained the best classification accuracy of 80.02% for negative, neutral, and positive valence using simple recurrent units (SRU) network.

As we mentioned, these above studies used 2D display as a visual display. Considering the differences in EEG dynamics between 2D and 3D presentations [28–30], the performances of these methods under a 3D environment are worthy of further evaluation. In this paper, motivated by the lack of public emotional datasets under the 3D presentation, we (1) developed a new emotional EEG dataset, named VREED, which adopted 3D VR videos as MIPs, and (2) provided a baseline performance of emotion recognition on the VREED.

## 3. Materials

### 3.1. Participants

Twenty-five participants (15 male, 10 female; mean age 22.92, SD 1.38 years) were enrolled from Shanghai University. All the participants reported no mental illness history and normal or corrected-to-normal vision. All participants signed informed consent before the experiment and got appropriate remuneration after the experiment. The experiment was approved by the Shanghai Ethics Committee for Clinical Research and followed the tenets of the Declaration of Helsinki.

### 3.2. Stimuli selection

Sixty 3D VR videos were produced by Shanghai film academy and shot at Shanghai landmarks (Oriental Pearl, the Bund, etc.), street scenes, and school theme parties using a Nokia OZO camera. Each video was 4-second long and encoded in H.264 format with a resolution of

$4096 \times 2048$  and 30 frames/second frame rate. We further divided these videos into positive, neutral, and negative categories (Fig. 1 according to valence [43], with 20 videos for each category to elicit positive, neutral, and negative emotions, respectively.

### 3.3. Emotion elicitation protocol

An HTC Vive VR headset was used to present all VR videos. The detailed protocol of emotion elicitation is shown in Fig. 2: (1) The 60 VR video clips were split into two groups, one group containing 20 positive and 10 neutral videos and another group containing 20 negative and 10 neutral ones. Considering the VR has a strong sense of immersion, we did not mix the negative and positive videos in one group, in order to reduce interference between different emotions. For each participant, the two video groups were displayed in random order, and the video clips within each group were also in random order. (2) Participants were given 3 min to relax before the experiment, 3 s of fixation cross hint preceded each video (those three seconds of brain electricity were used as the baseline), and a rest time to calm down after each group. (3) After each video, participants were asked to rate the emotional valence induced by the video. And (4) the two groups of video clips were played twice. Therefore, there were  $60 * 2 = 120$  EEG trials for each participant. The experimental environment is shown in Fig. 3.

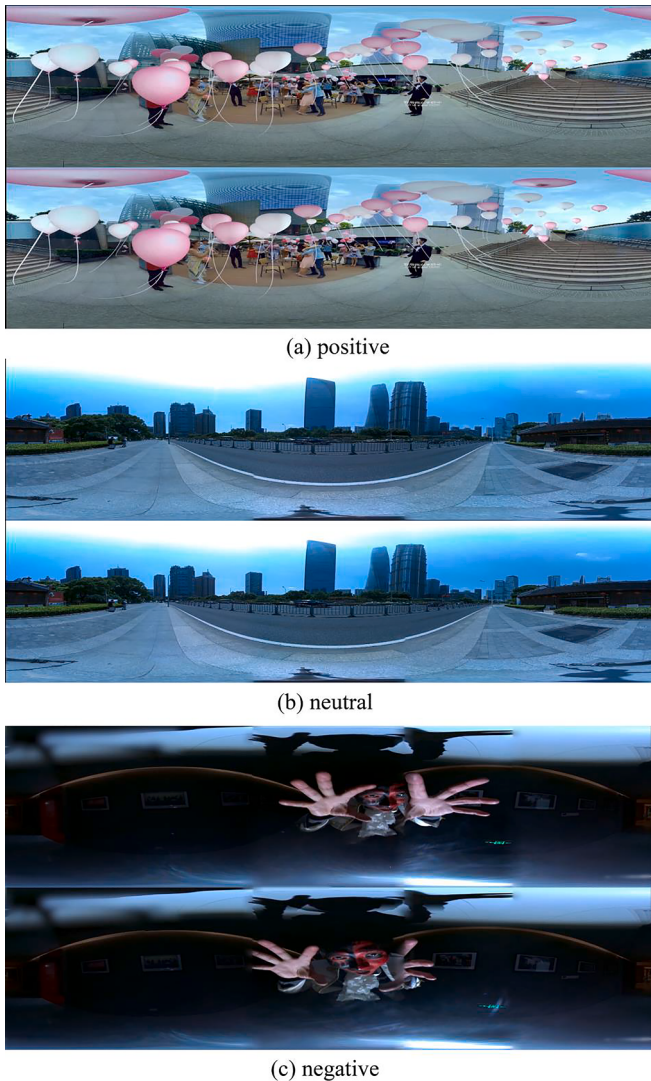


Fig. 1. Snapshots from the three categories of binocular 3D VR videos.

### 3.4. EEG recording and pre-processing

EEG recordings were collected during the participants' watching VR videos using a 64-channel wireless EEG device (Neuracle Technology, Changzhou, China) at a 1000 Hz sampling rate, and impedances were kept below  $5\text{ k}\Omega$ . Fifty-nine data electrodes positioned in five brain regions (occipital, parietal, frontal, right temporal, and left temporal) were selected from the 64 electrodes based on an extended International 10–20 system (10–10 system) [44], as shown in Fig. 4. The EEGLab Toolbox [45] was used to pre-process all the collected EEG recordings offline, including removing artifacts and power frequency interference, baseline adjustment, cutting bad trials, etc. Six of the 25 participants were excluded from the dataset due to poor data quality, and the valid participants were 19 (13 male, 6 female; mean age 22.84, SD 1.50 years). The comparison of emotion datasets mentioned above is shown in Table 1: (1) only the VREED and the dataset in literature [1] are used VR as MIPs; and (2) Compared to the literature [1], VREED used higher density EEG electrodes, which are more conducive to get a full range of spatial detail in the brain's electrical fields [32].

## 4. Methods

### 4.1. EEG feature extraction

Previous studies have shown that feature extraction is one of the most critical phases in EEG-based emotion classification because different feature extraction methods may significantly impact classification performance. The primary purpose of feature extraction is to find the most compacted and informative EEG data representation to map the EEG to emotional states. We first decomposed the preprocessed EEG data into four sub-frequency bands, namely: theta (4–8 Hz), alpha (8–13 Hz), beta (13–30 Hz), and gamma (30–49 Hz), and then extracted the spectral power and topological properties of functional brain networks from each sub-frequency band as classification features.

#### 4.1.1. Spectral power features

EEG spectral power can be analyzed to characterize the local brain activations [20]. In this study, we estimated the relative power of each sub-frequency band and the inter-hemispheric power indices as classification features.

(1) The relative power denotes the relative contribution of each sub-frequency power to the total power, which could decrease the differences between the subjects comparing with absolute power [46]. Both non-parametric spectral estimators (Welch, multitaper, etc.) [23,47] and parametric spectral estimation (modified covariance, Burg, etc.) [48] are widely used in EEG power estimating. We used the Welch method in this paper, and the calculation of the relative power can be calculated as follows:

a) Estimating power spectral density (PSD) using the Welch average periodogram algorithm. Given a time series  $x$ , Welch's method first divided the series  $x$  into  $L$  data segments with each data segment containing  $K$  data samples and then performed the periodogram for each segment and averaging (here,  $K$  equals 500, which is the product of 0.5 (window size) and 1000 (sampling rate), and with overlapping of 50%). For the  $m^{\text{th}}$  segment  $x_m(n)$ , its periodogram can be defined as:

$$PSD_m(f) = \frac{1}{K} \left| \sum_{n=0}^{K-1} x_m(n) w(n) e^{-j2\pi f n} \right|^2, \quad (1)$$

where  $w(n)$  is a window function to reduce spectral leakage effects, and  $j$  is the imaginary unit. Then the Welch estimate of the Power spectral density is presented as follows:

$$PSD = \frac{1}{L} \sum_{i=0}^{L-1} PSD_i(f) \quad (2)$$

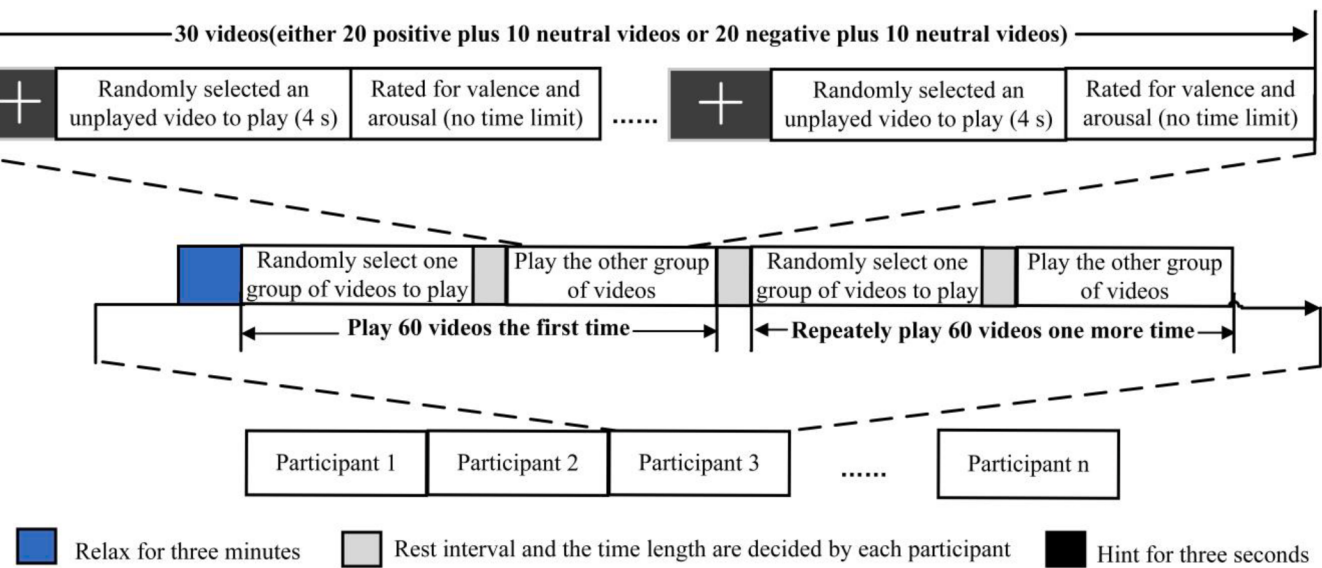


**Fig. 2.** Protocol of emotion elicitation experiment.



**Fig. 3.** Photograph of the experimental environment.

- b) Calculating the area under the *PSD* curve corresponding to some specific sub-frequency band as the absolute Power with Simpson's rule.
- c) Estimating relative band powers of each frequency band for each trial by the formula:

$$RP(f_i, f_h) = \frac{P(\text{Selecting range})}{P(\text{Total range}(4 \sim 49\text{Hz}))}, \quad (3)$$

where  $RP(\cdot)$  represents the relative power,  $P(\cdot)$  indicates the absolute power obtained in step b).

(2) Previous studies have reported the phenomenon of inter-hemispheric EEG power asymmetry in emotion processing [49–51]. In this study, the inter-hemispheric power indices were extracted as classification features. There were twenty-six asymmetry indices resulted from twenty-six symmetric electrode combinations across the whole brain, namely AF3-AF4, AF7-AF8, F1-F2, F3-F4, F5-F6, F7-F8, Fp1-Fp2, FC1-FC2, FC3-FC4, FC5-FC6, C1-C2, C3-C4, C5-C6, CP1-CP2, CP3-CP4, CP5-CP6, P3-P4, P5-P6, P7-P8, FT7-FT8, T7-T8, TP7-TP8, PO3-PO4, PO5-PO6, PO7-PO8, O1-O2. The asymmetry indices could be calculated either by relative power division or subtraction and named rational asymmetry (RASM) and differential asymmetry (DASM) features, as formulas (4) and (5).

$$RASM = RP(\text{left})/RP(\text{right}) \quad (4)$$

$$DASM = RP(\text{left}) - RP(\text{right}) \quad (5)$$

#### 4.1.2. Spearman correlation topological graph

The VREED dataset was collected from a 59-channel EEG device and had 2043 trials. We calculated the Spearman correlation between the sub-frequency band RP of each channel and the ratings of video valence. Taking the theta band as a sample, we illustrate the detailed calculation procedure as follows:

- Estimating relative power for each trial, each channel and got a 2043(row) by 59(column) RP matrix,  $M_{2043 \times 59}$ .
- Performing the Spearman correlations between each column of  $M$  and all valence ratings (2043 trials), as shown in Fig. 5.
- Plotting the topological graph according to 59 Spearman correlation coefficients obtained in step b).

#### 4.1.3. Functional brain network features

Studies have shown that functional connectivity and interaction can effectively represent the brain's comprehension of emotion induced by auditory-visual stimuli among relevant brain networks [20]. Phase synchronization of oscillatory neuronal populations has been found to exist in the processes of cognitive dynamics widely. It underlies some influential theories, such as 'Binding by synchrony theory [52,53]' and 'Communication through coherence' (CTC [54]). Moreover, many studies have noted that synchrony measures are more discerning based on the phase information than amplitude information [20,55]. Therefore, the phase locking value (PLV) was used to describe the non-linear phase relationship between different brain regions. Similarly, we constructed brain networks of different frequency bands for each trial. Given a brain network it can be constructed as follows: (1) defining 59 nodes in the network, each node corresponding to a channel on the scalp (Fig. 4), (2) estimating the functional connectivity using PLV between every possible channel pair, which generated a 59 by 59 symmetric matrix, and (3) converting the functional connectivity matrix into a brain network using minimum spanning tree (MST) method.

#### Phase locking value

The PLV was used to calculate functional connectivity for every possible channel pair, which is defined as [56]:

$$\text{PLV} = \frac{1}{N} \left| \sum_{t=1}^N e^{i(\theta_1(t) - \theta_2(t))} \right|, \quad (6)$$

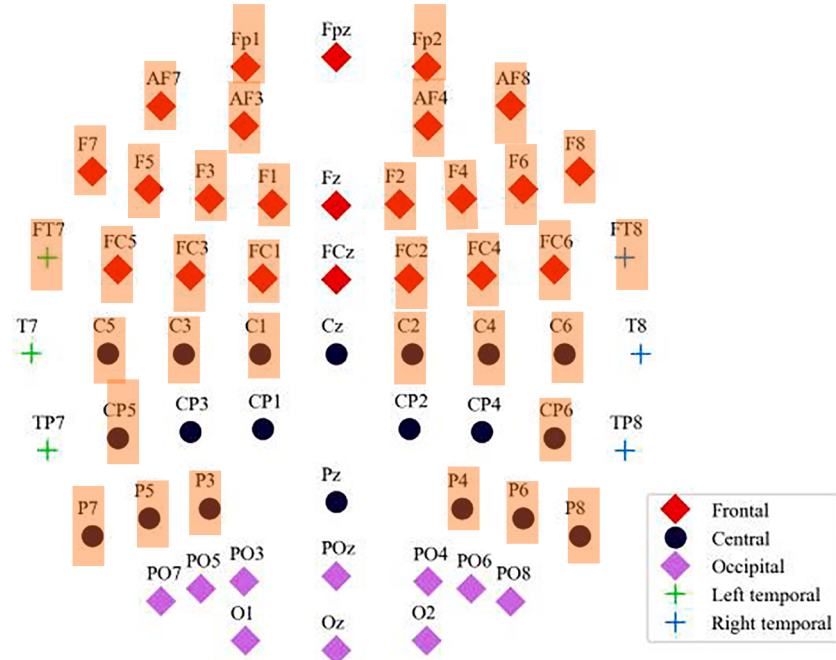


**Fig. 4.** Position of fifty-nine data electrodes based on an extended International 10–20 system (10–10 system).

**Table 1**  
Comparison of EEG datasets mentioned above.

Dataset	MIPs	EEG channels	Participants	Number of trials	Trial length
MAHNOB-HCI [22]	Twenty 2D videos in the 1st experiment	32	27 (11 male and 16 female)	540	Between 34.9 and 117 s long (mean = 81.4, std = 22.5 s)
DEAP [23]	Forty 2D music videos	32	32 (50% female)	1280	60 s
SEED [17]	Fifteen 2D video clips	62	15 (7 male and 8 female)	675	About 240 s
Literature [1]	Four VR scinareos	9	38 (39% male, 61% female)	152	90 s
Our dataset (VREED)	Sixty 3D VR videos	59	19 (13 male, 6 female)	2043	4 s

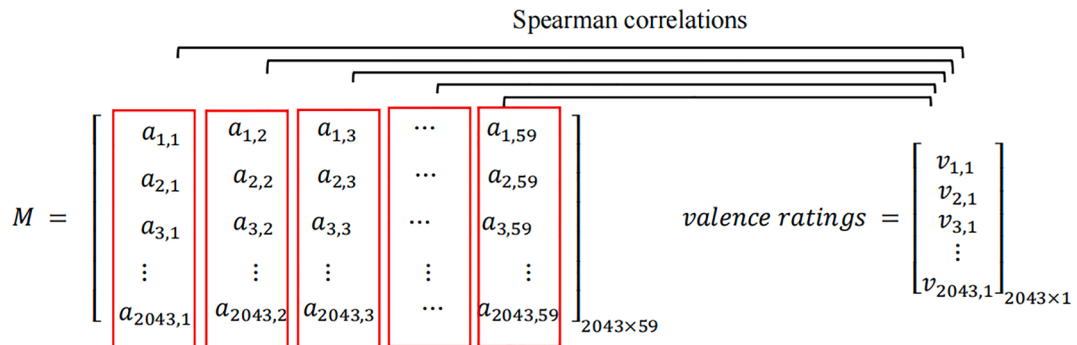


**Fig. 5.** The procedure of calculating Spearman correlation. For each sub-frequency band, 59 correlation coefficients can be obtained, one for each channel.

where  $N$  is the total number of sampling points;  $\theta_i(t)$  represents the instantaneous phase value of the  $i^{th}$  ( $i = \{1, 2\}$ ) time series at the time point  $t$ , which is estimated by the formula (7):

$$\theta_i(t) = \arctan \frac{\tilde{x}_i(t)}{x_i(t)}, \quad (7)$$

where  $\tilde{x}_i(t)$  denotes the Hilbert transform of time series  $x_i(t)$  (in our case, an EEG time series of a specific band). The Hilbert transform of a discrete-time signal  $x(t)$  could be directly extracted from the analytic

signal  $x_a(t)$ , as the formula (8) [57,58].

$$x_a(t) = F^{-1}(F(x(t))2U) = x(t) + \tilde{x}(t) \quad (8)$$

where  $F$  is the Fourier transform,  $F^{-1}$  the inverse Fourier transform,  $U$  the unit step function,  $j$  the imaginary unit, and  $\tilde{x}(t)$  the Hilbert transform of  $x(t)$ .

We further calculated the mean PLV (MPLV) for each channel as a classification feature. Given a channel, its mean PLV was calculated by averaging the PLV value over all its connected channels [59]. The larger

the mean PLV of a channel is, the stronger the functional connection between the channel with others is.

#### MST algorithm

The MST algorithm was applied to convert each PLV matrix to an undirected binary graph representation of the functional brain network. Given a PLV matrix, the details of the MST algorithm could be described as follows [60,61]: (1) sort all functional connectivities of the matrix in descending order; (2) Link the nodes with maximal functional connectivity until all the nodes are linked in an acyclic subgraph; (3) Skip the functional connectivity if the addition of it leads to a cycle. Compared to the traditional method of converting a matrix to a binary network by setting a threshold, the MST can preserve the brain network structure and avoid arbitrary threshold selection [61]. Further, betweenness centrality (BC) and nodal efficiency (NE) of the functional networks be extracted by graph theory as classification features.

Let  $G(V, E)$  be an undirected binary-valued brain network with a set of nodes  $V(V \neq \emptyset)$  and links  $E(E \neq \emptyset)$ . The definitions of betweenness centrality and nodal efficiency are briefly described as follows.

*Betweenness centrality* measures the extent to which a vertex lies on paths between other vertices. For a specific node  $j$ , its betweenness centrality  $c_B(j)$  is the sum of the fraction of all-pairs shortest paths that pass through  $j$  [62]:

$$c_B(j) = \sum_{s,t \in V} \frac{\sigma_{st}(j)}{\sigma_{st}}, \quad (9)$$

where  $\sigma_{st}$  is the total number of shortest paths from node  $s$  to node  $t$ , and

$\sigma_{st}(j)$  is the number of those paths passing through the node  $j$  other than  $s, t$ . If  $j \in s, t$ ,  $\sigma_{st}(j) = 0$  and if  $s = t$ ,  $\sigma_{st} = 1$  [63].

*Nodal efficiency* measures information propagation between a node and the remaining nodes in the network [64]. For a specific node  $j$ , its nodal efficiency  $e_j$  is calculated as the formula (10) [30]:

$$e_j = \frac{1}{N-1} \sum_{k \neq j \in V} \frac{1}{d_{jk}}, \quad (10)$$

where  $d_{jk}$  is the shortest path length between nodes  $j$  and  $k$ ; we set  $N = |V|$  in this work.

#### 4.2. Feature selection

Feature selection can not only improve classification performance but also reduce time consumption. In this study, the feature selection was performed using a random forest classifier implemented with the Python package scikit-learn [65], which could compute impurity-based feature importances. Specifically, each feature's Gini importance (or mean decrease impurity) was computed in creating a random forest model. A feature's Gini importance in a single tree was calculated by adding the Gini index reduction (from parent to children) brought by the feature. And a feature's Gini importance in the random forest was defined as the average Gini importance across all trees. Features with higher Gini importance indicate that they are more important in the classification.

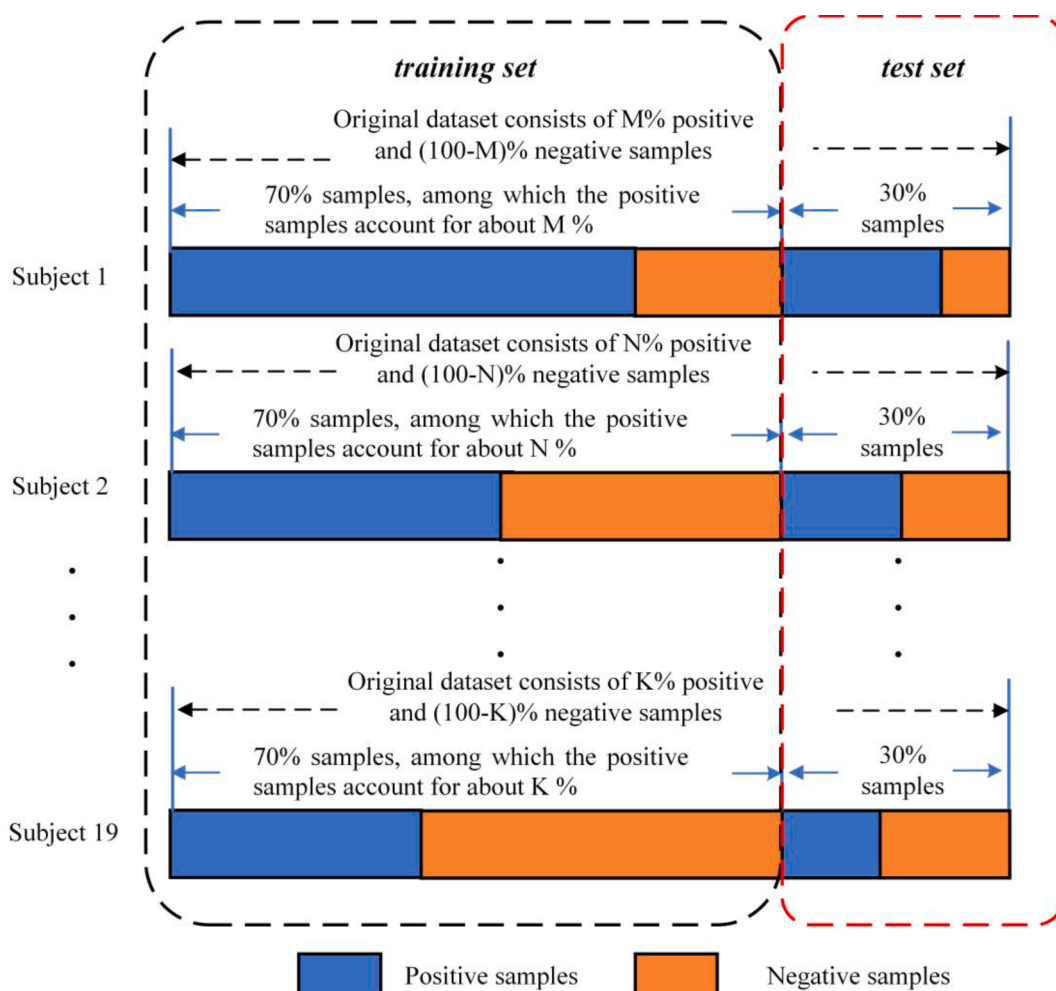


Fig. 6. Division of the VREED dataset used for training and test.

#### 4.3. Emotional state classification

We treated every EEG trial as a classification sample and performed two-class emotion classification (only negative and positive samples) using the EEG power and brain network features. A support vector machine (SVM) classifier was used to assess the association between emotional states and EEG. First, we divided the samples of each participant into 70% training set and 30% test set, keeping the percentage of each class in the training and testing sets approximately the same as the original dataset (Fig. 6). Then, the training sets of all subjects were combined as the final training set to train the SVM classifier. Finally, the test sets of all participants were combined as the final test set to evaluate the classifier performance. Classification accuracy was regarded as the primary performance indicator. Additionally, in order to reduce the classification performance's randomness caused by the dataset's random division, the classification procedure was repeated 10 times, and the average classification performance was calculated.

## 5. Results

### 5.1. Behavioral results

Table 2 shows the participants' valence ratings of 20 positive, neutral, and negative VR videos, respectively. The positive VR videos obtained the highest valence rating, the negative the lowest, and the neutral between the positive and the negative, which indicated that the chosen VR videos successfully elicited desired emotions.

Subsequently, participants' valence ratings to the videos were used as ground truth to label EEG trials. Trials with a valence score less than five were labeled as negative, equal to five were neutral, and greater than five were positive. After the preprocessing, the negative, neutral, and positive trial numbers are 696, 637, and 710, respectively. Each trial was used as a sample in the following classification processes.

### 5.2. Correlates of EEG relative power and valence

Fig. 7 shows the topological maps of averaged relative power across trials for negative, neutral, and positive emotional states. It showed that the power distribution in the same frequency band was similar across the three emotional states.

Further, The Spearman correlation coefficients were calculated between channel power changes and valence ratings, as shown in Fig. 8 and Table 3. The significance level was set to 0.001, a much smaller value than the commonly used 0.05, to low the probability of the type I error caused by multiple correlations. We observed that (1) the occipital power of theta and alpha bands was positively correlated with the valence ratings; the occipital power of beta and gamma bands was negatively correlated with valence ratings, and (2) the left frontal power of the theta and alpha bands was negatively correlated with the valence ratings; the left frontal power of the beta and gamma bands was positively correlated with valence ratings.

### 5.3. Emotion classification with different features

In this paper, we are mainly interested in classifying negative and positive emotional states. We extracted the RP, RASM, DASM, MPLV, BC, and NE from EEG time series as classification features, and the classification accuracy was adopted as a primary performance indicator.

**Table 2**  
Participants' valence rating for positive, neutral, and negative VR videos.

Pairwise	Mean (SD)	P-value (10,000 permutation tests)
Positive / neutral	6.41(1.26)/5.20 (0.87)	< 0.001
Positive/ negative	6.41(1.26)/ 2.72 (1.30)	< 0.001
Neutral /negative	5.20 (0.87)/ 2.72 (1.30)	< 0.001

Table 4 shows average classification accuracies of RP, RASM, DASM features across the theta, alpha, beta, gamma, and ALL frequency bands. We found that: (1) the classification accuracies of theta and gamma bands are higher than that of the alpha and beta bands under the same feature type; for example, for the RP features, the theta and gamma band obtain the classification accuracies of  $71.35\% \pm 2.01\%$  and  $68.30\% \pm 2.01\%$ , higher than that of alpha and beta bands which are  $65.56\% \pm 2.13\%$  and  $63.14\% \pm 1.90\%$ ; (2) Feature combination of four frequency bands can improve classification accuracy; i.e., the ALL frequency band holds the highest classification accuracy for the same feature; and (3) The RP feature obtains higher classification accuracies than the RASM and DASM features for the same frequency band.

Since the RP feature has the highest classification accuracy among the three types of features, we further calculated the confusion matrices of RP features in different frequency bands, as shown in Fig. 9.

Subsequently, the brain network indices MPLV, BC, and NE were calculated as classification features. The average classification accuracies of MPLV, BC, and NE features showed that (Table 5): (1) the classification accuracies of beta and gamma bands are higher than that of the theta and alpha bands under the same feature type; for example, for the MPLV features, the beta and gamma band obtain the classification accuracies of  $62.53\% \pm 3.25\%$  and  $66.70\% \pm 2.80\%$ , higher than that of theta and alpha bands which are  $57.63\% \pm 2.79\%$  and  $57.47\% \pm 0.93\%$ ; (2) Feature combination of four frequency bands can improve classification accuracy; i.e., the ALL frequency band holds the highest classification accuracy for the same feature; and (3) The MPLV feature obtains higher classification accuracies than the BC and NE features for the same frequency band.

Since the MPLV feature has the highest classification accuracy among the three types of features, we further calculated the confusion matrices of the MPLV feature in different frequency bands, as shown in Fig. 10.

The highest accuracy was  $73.77\% \pm 2.01\%$  from the above-mentioned results, obtaining using the RP feature of ALL frequency band for the negative/positive emotion classification.

### 5.4. Effects of feature selection on classification performance

Feature selection can not only improve prediction performance but also reduce time consumption. In this study, feature selection was performed using a random forest classifier to select an optimal subset of features. Feature selection was based on the RP feature of ALL frequency band due to the highest classification accuracy was obtained using it. The feature selection process is as follows.

- (1) Split the original dataset into a 70% training set and 30% testing set.
- (2) Fitted a random forest classifier on the training data to compute the Gini importance of each feature.
- (3) Trained SVM classifiers with the top n (from 5 to 236 with a step size 5) feature(s) in the training set and estimated the classification performance on the test set with the trained SVM.
- (4) Repeated step (1) ~ (3) 10 times and calculated the average classification accuracy and Gini importance.

The classification performance using top n (from 5 to 236 with a step size 5) features is shown in Fig. 11. From Fig. 11, using the top 35 features, the average classification accuracy was 71.95%, higher than 71.35%—the highest classification accuracy obtained by the RP features of the individual frequency band and the latter's feature dimensionality is 59.

Further, averaged Gini importance of each feature was obtained by the average across 10 repetitions. The distribution of the top 35 features as shown in Fig. 12, we found: (1) the selected features are primarily located in occipital and frontal regions, which in line with the correlation results of EEG power and valence (Fig. 8), and (2) most of the

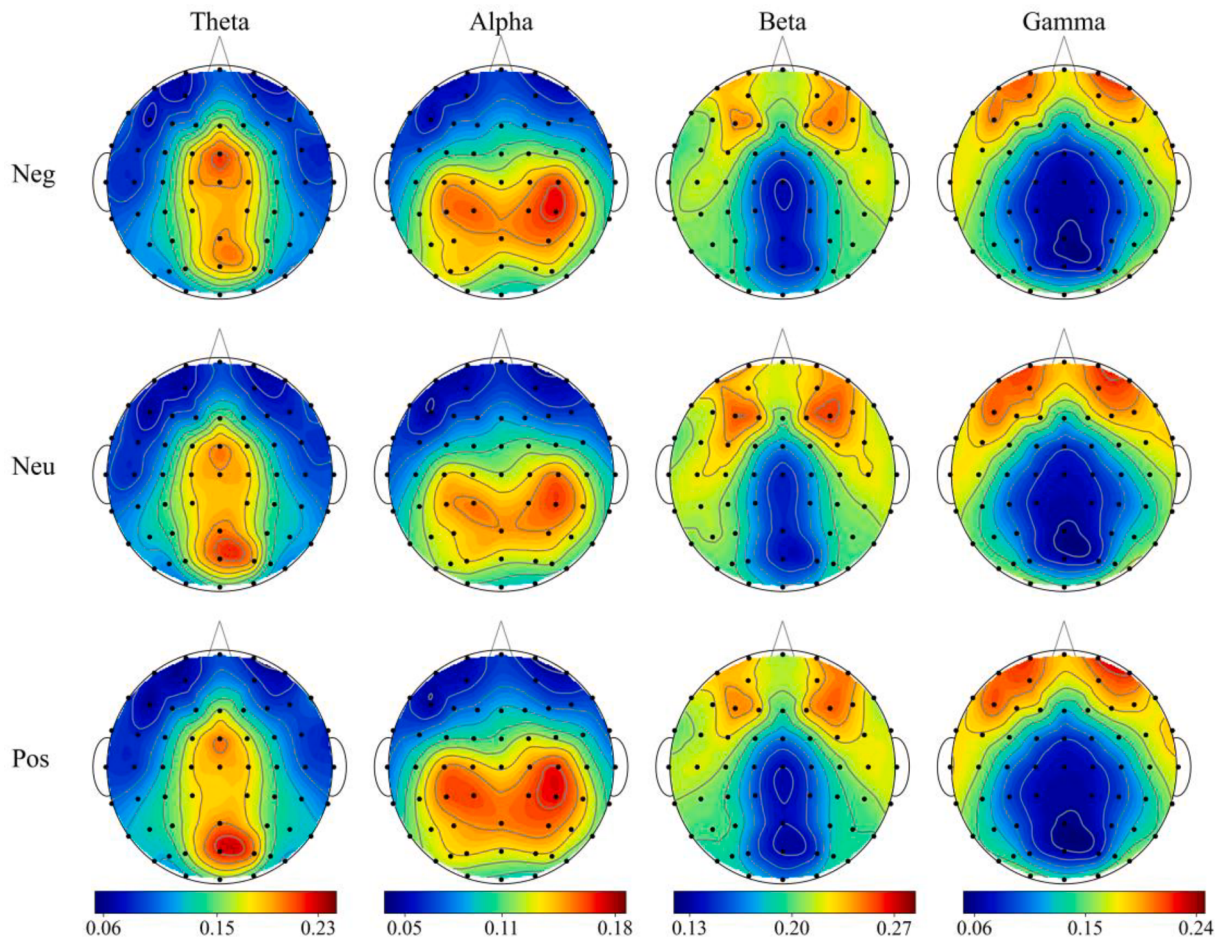


**Fig. 7.** The averaged relative power topological graphs across subjects under different emotional states.

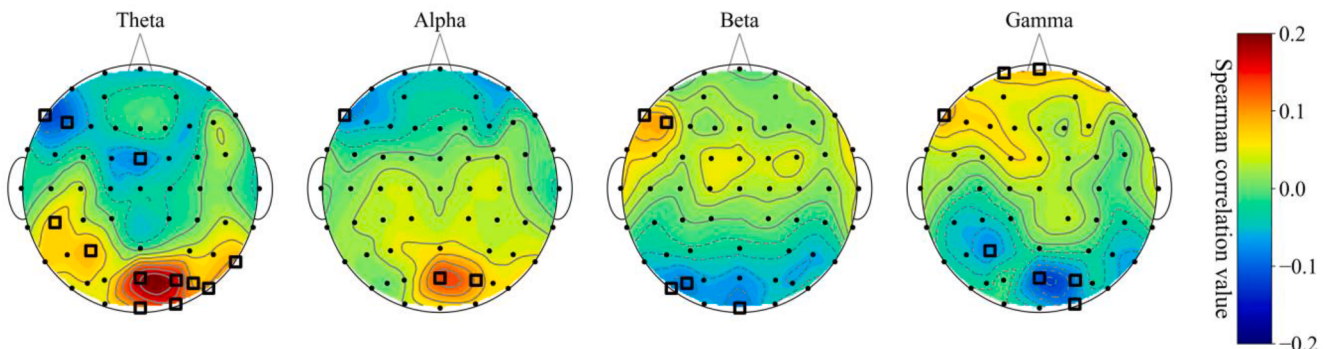


**Fig. 8.** Topological graphs of the Spearman correlations between valence ratings and relative power. Channels with square markers indicate Spearman p-value  $<0.001$ .

selected features came from the theta and gamma bands, which might explain the higher classification accuracies obtained by using the theta and gamma band RP features compared with the alpha and beta band RP features (Table 4).

## 6. Discussion

Many previous EEG-based emotion recognition experiments used 2D pictures and videos as emotion eliciting materials. However, studies based on 2D stimuli might obtain poor application effects on the real 3D world [28]. Therefore, increasing researchers recommended using 3D VR as MIPs in emotion-related studies, allowing researchers to simulate

environments in controlled laboratory conditions with a high sense of presence and interactivity [2]. Up to now, to our knowledge, only one public emotion EEG dataset has used VR scenarios as MIPs [1], partly due to the relative complexity of VR production. This paper develops a new emotion EEG dataset, which, to our knowledge, is the first high-density emotion EEG dataset with 3D VR videos as MIPs. The permutation test results of behavioral data (Table 2) confirmed that VR could effectively induce specific emotions as introduced in other literature [1,66].

Furthermore, we performed negative/positive valence classification in the new dataset based on power and network features. We obtained the highest accuracy of  $73.77\% \pm 2.01\%$  using the combined features of

**Table 3**

EEG channels with Spearman p-value &lt;0.001 across different frequency bands.

Theta			Alpha			Beta			Gamma		
Ch.	CC.	p-value	Ch.	CC.	p-value	Ch.	CC.	p-value	Ch.	CC.	p-value
F5	-0.0955	$1.54 \times 10^{-5}$	F7	-0.0867	$8.72 \times 10^{-5}$	F5	0.0863	$9.34 \times 10^{-5}$	Fpz	0.0819	$2.09 \times 10^{-4}$
F7	-0.1241	$1.83 \times 10^{-8}$	POz	0.1323	$1.93 \times 10^{-9}$	F7	0.0845	$1.32 \times 10^{-4}$	Fp1	0.0739	$8.30 \times 10^{-4}$
FCz	-0.0752	$6.69 \times 10^{-4}$	PO4	0.0957	$1.48 \times 10^{-5}$	PO5	-0.0891	$5.55 \times 10^{-5}$	F7	0.0935	$2.32 \times 10^{-5}$
CP5	0.0728	$9.91 \times 10^{-4}$				PO7	-0.0807	$2.62 \times 10^{-4}$	P3	-0.0738	$8.41 \times 10^{-4}$
P3	0.0847	$1.28 \times 10^{-4}$				Oz	-0.0941	$2.03 \times 10^{-5}$	POz	-0.1114	$4.45 \times 10^{-7}$
P8	0.0944	$1.92 \times 10^{-5}$							PO4	-0.0829	$1.77 \times 10^{-4}$
POz	0.1770	$7.76 \times 10^{-16}$							O2	-0.0769	$5.04 \times 10^{-4}$
PO4	0.1638	$9.26 \times 10^{-14}$									
PO6	0.0866	$8.92 \times 10^{-5}$									
PO8	0.0960	$1.39 \times 10^{-5}$									
Oz	0.1008	$4.95 \times 10^{-6}$									
O2	0.1336	$1.33 \times 10^{-9}$									

Note: 'Ch.' represents EEG channels, 'CC.' represents the Spearman correlation coefficient, and 'p-value' indicates the Spearman p-value.

**Table 4**

Average classification accuracies of RP, RASM, and DASM features. (Unit: %)

Spectral features (mean $\pm$ S.D.)	EEG frequency band				
	Theta	Alpha	Beta	Gamma	ALL*
RP	71.35 $\pm$ 65.56 $\pm$ 63.14 $\pm$ 68.30 $\pm$ 73.77 $\pm$ 2.01				
		2.13	1.90	2.01	2.01
RASM	62.95 $\pm$ 59.14 $\pm$ 58.14 $\pm$ 63.72 $\pm$ 68.28 $\pm$ 2.22				
		1.45	1.74	1.58	1.54
DASM	64.47 $\pm$ 60.21 $\pm$ 57.72 $\pm$ 62.16 $\pm$ 68.35 $\pm$ 2.10				
		3.15	1.62	2.25	1.50

\*Note: Here, 'ALL' means concatenating the theta, alpha, beta, and gamma band features.

the theta, alpha, beta, and gamma relative power. In addition, several significant findings can be drawn from our study: (1) for the power features, the theta and gamma bands achieved higher classification performance than the alpha and beta bands (Table 4); for the network features, the beta and gamma bands achieved higher classification performance than the theta and alpha bands (Table 5); and (2) The occipital and frontal EEG relative power contain important information related to emotion.

### 6.1. VR EEG features on emotion processing

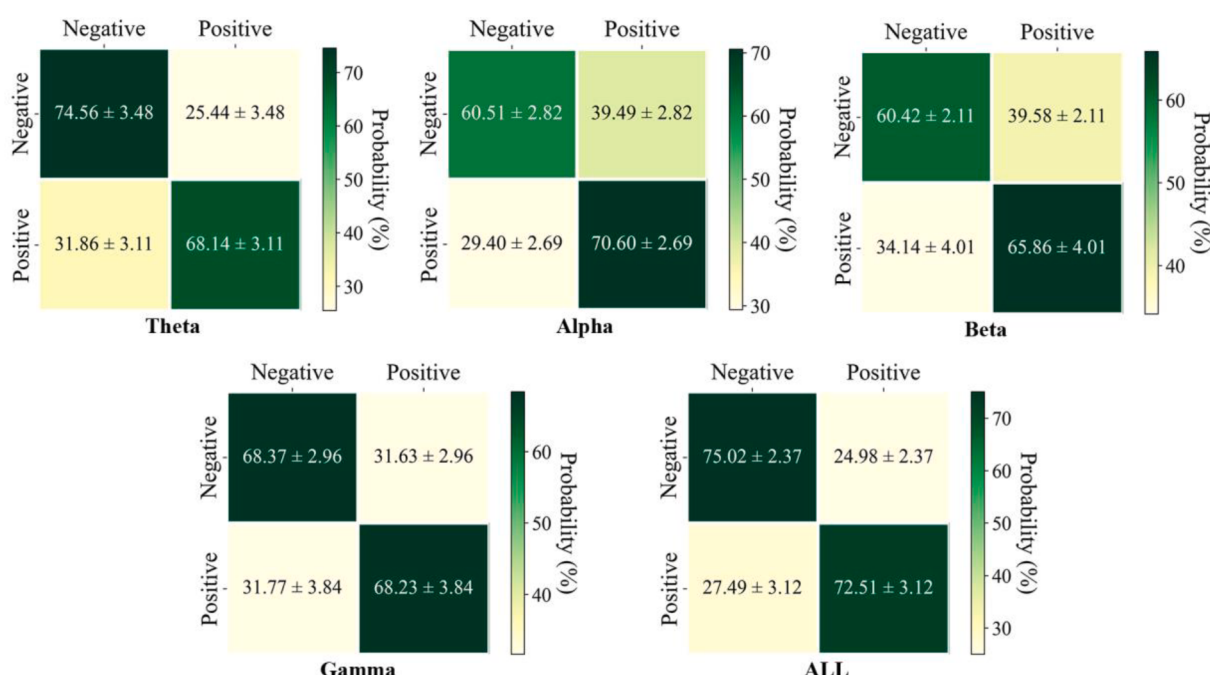
For the power features RP, RASM, and DASM, the average classification accuracies of the theta and gamma bands were higher than that of the alpha and beta bands, indicating that the theta and gamma power contained more information about emotion processing. Previous studies have investigated theta oscillatory responses on the presentation of 2D emotional video clips and the International Affective Picture System

**Table 5**

Average classification accuracies of MPLV, BC, and NE features. (Unit: %)

Network features (mean $\pm$ S.D.)	EEG frequency band				
	Theta	Alpha	Beta	Gamma	ALL
MPLV	57.63 $\pm$ 57.47 $\pm$ 62.53 $\pm$ 66.70 $\pm$ 67.91 $\pm$ 2.79				
		0.93	3.25	2.80	2.77
BC	55.51 $\pm$ 54.79 $\pm$ 58.28 $\pm$ 60.23 $\pm$ 61.40 $\pm$ 1.58				
		2.26	2.53	2.06	1.70
NE	56.40 $\pm$ 55.56 $\pm$ 58.63 $\pm$ 62.65 $\pm$ 63.09 $\pm$ 2.47				
		1.96	2.30	2.20	2.04

Note: Here, 'ALL' means the concatenation of theta, alpha, beta, and gamma band features.

**Fig. 9.** Averaged confusion matrices for 10 repetitions of classification using the RP feature.

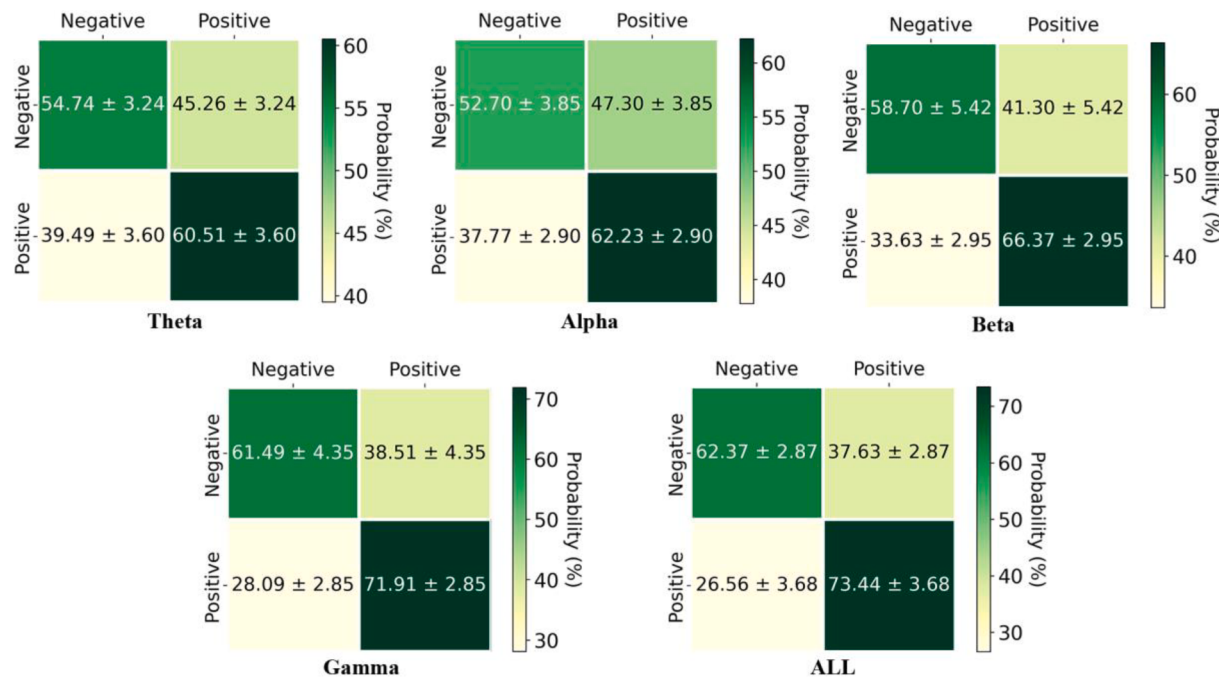


Fig. 10. Averaged confusion matrices for 10 repetitions of classification using the MPLV features.

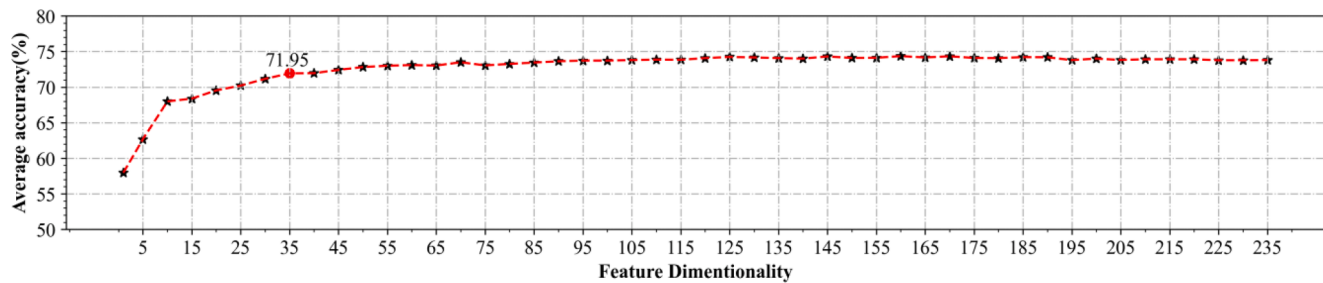


Fig. 11. The average classification accuracies of different feature dimensionality.

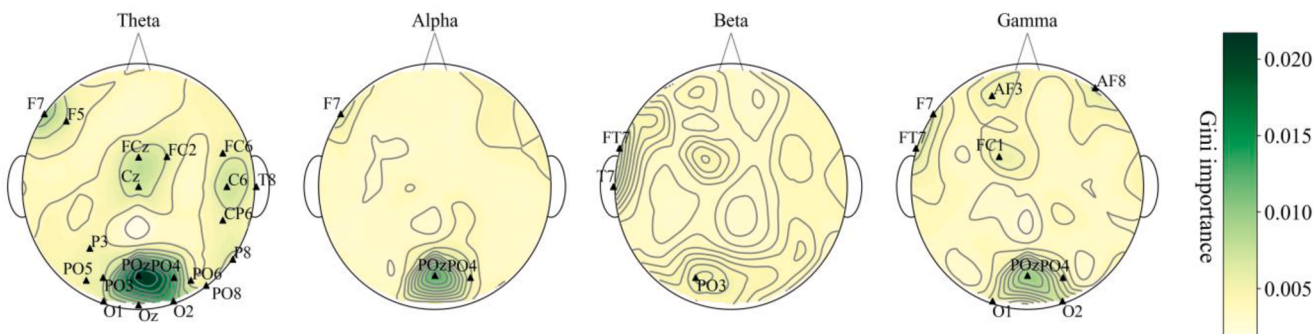


Fig. 12. Distribution of the top 35 RP features selected using the random forest classifier.

(IAPS) pictures. For example, Aftanas et al. reported [67] that positive videos increased theta power compared to neutral videos; however, negative videos caused a decreased theta power. We observed that (1) the occipital and frontal theta power are quite different in negative and positive emotional states from feature selection (Fig. 12); and (2) From Spearman correlation analysis (Fig. 8), a decreased valence induced a decreased occipital theta power (positive correlation) and an increased frontal theta power (negative correlation). Because the theta power is associated with attention [68,69], we think our findings are related to

attention differences paid to different valence videos. Previous studies have demonstrated that the negative stimuli have more informational value than positive ones, necessitating more attention and cognitive processing [70,71]. Moreover, the occipital theta power was positively correlated with the valence rating (Fig. 8), in line with previous results gained from the DEAP dataset [23].

Research demonstrated that gamma activity widely existed in the central nervous system, including regions linked with emotional processing, for example, the perirhinal cortex and amygdala [72,73]. We

observed that (1) the occipital and frontal gamma power are quite different in negative and positive emotional states from feature selection (Fig. 12); and (2) From Spearman correlation analysis (Fig. 8), a decreased valence caused an increased occipital gamma power (negative correlation) and a decreased frontal gamma power (positive correlation). EEG gamma oscillations were correlated to visual cognition, such as video watching, visual awareness, visual short-term memory maintenance, and object-based attention [74,75]. The negative VR videos needed more cognitive processing than the positive ones [70,71], which may lead to gamma power differences between the positive and negative emotional states. Therefore, the potential power differences of the theta and gamma bands in different emotional states may obtain higher accuracy based on the power of these two sub-frequency bands.

In addition, some previous studies reported that the beta and gamma power showed more information about emotion processing. For example, Li et al. [20] reported that when adopted SVM classifier and F-score feature selection, the beta and gamma PSD features obtained higher accuracy than theta and alpha PSD features on the DEAP, MAHNOB, and SEED datasets. We think that the differences with our results that the theta and gamma power contained more information about emotion processing may be related to different MIPs and is worthy of further study.

For the network features MPLV, BC, and NE, we observed that the average classification accuracies of the beta and gamma bands were higher than that of the alpha and theta bands (Table 5). This is different from the higher classification accuracies obtained by the power features of the theta and gamma bands, indicating that different feature extraction methods may affect emotion recognition performance for the same frequency band. In addition, we achieved relatively high classification accuracy using both the power features and the brain network features of the gamma band, indicating that the gamma band owns a more stable ability in emotion recognition.

## 6.2. The influence of the features from different brain regions on classification

We obtained consistent results from the Spearman correlation analysis (Fig. 8) and random-forest-based feature selection (Fig. 12) that the electrodes located in the frontal and occipital regions played a more important role in emotion recognition. Previous studies have shown that the frontal area dominantly contributed to emotion perception and recognition [76–78]. For example, Heberlein et al. [77] reported that the ventromedial frontal cortex plays a crucial role in facial emotion recognition. Coan et al. [51] reported that positive emotions are associated with relatively greater left frontal brain activity, whereas “withdrawal” emotions are associated with relatively greater right frontal brain activity. Because the frontal lobe is important in emotional processing, emotion recognition based on only the frontal EEG signals has been widely studied. For example, Wu et al. [79] classified low/high valence using features extracted from two frontal EEG channels FP1 and FP2, obtaining a mean classification accuracy of 75.18% on the DEAP dataset. Moreover, the occipital lobe is involved in visual processing [80,81], and previous studies have demonstrated that emotional processing closely interacts with attentional functions [70,71]. In this study, the VR videos of different valences may lead to differences in participant’s attention, which is likely to be reflected in the occipital EEG signals.

We selected the most important features and eliminated features with high correlation using a random forest classifier, which could calculate impurity-based feature importance and, in turn, can be used to eliminate unnecessary features [65]. The random-forest-based feature selection has the advantages of (1) easy parallelization and computation [82] and (2) considering the interaction between features when determining the importance of features [83]. As a result, random forest is particularly well suited to high-dimensional feature space, for example, the biomedical field [82,84,85].

Last but not least is the choice of power spectrum estimation methods. Alkan et al. [86] reported consistently superior performance of the covariance methods over Welch and Yule-Walker methods in EEG-based epileptic seizure detection. However, there is no study that tells us which estimation method is best for the EEG-based emotion recognition, that deserves further investigation.

## 7. Conclusion

In this paper, we studied EEG-based emotion recognition in a virtual reality environment. We first developed a new public emotional EEG dataset, VREED, which uses 3D VR videos as MIPs. Then, spectral power (RP, RASM, DASM) and brain network (BC, NE, and MPLV) features were extracted to perform the negative/positive valence recognition, providing a baseline classification performance on the VREED dataset. We believe that the VREED dataset, which uses 3D VR videos as MIPs, can provide emotional EEG data similar to the real-world situation and consider further expanding the sample size of the VREED dataset in the future.

### Data availability

The VREED data used to support the findings of this study are currently under embargo. Six months after the publication of this article, requests for data will be considered by the corresponding author under license agreement.

### Funding

This work was funded by the National Social Science Fund of China (NO.17BC043).

### Declaration of Competing Interest

The authors declare that they have no known competing financial interests or personal relationships that could have appeared to influence the work reported in this paper.

### Acknowledgments

We would like to express our gratitude to Haibao Li for collecting EEG data.

### References

- [1] J. Marín-Morales, J.L. Higuera-Trujillo, A. Greco, J. Guixeres, C. Llinares, E. P. Scilingo, M. Alcañiz, G. Valenza, Affective computing in virtual reality: emotion recognition from brain and heartbeat dynamics using wearable sensors, *Sci. Rep.* 8 (2018) 1–15.
- [2] N.S. Suhaimi, J. Mountstephens, J. Teo, EEG-based emotion recognition: A state-of-the-art review of current trends and opportunities, *Comput. Intell. Neurosci.* 2020 (2020) 1–19.
- [3] H. Huang, Q. Xie, J. Pan, Y. He, Z. Wen, R. Yu, Y. Li, An EEG-based brain computer interface for emotion recognition and its application in patients with Disorder of Consciousness, *IEEE Trans. Affect. Comput.*, 2019.
- [4] H. Yoon, S.-W. Park, Y.-K. Lee, J.-H. Jang, Emotion recognition of serious game players using a simple brain computer interface, in: 2013 Int. Conf. ICT Converg., IEEE, 2013: pp. 783–786.
- [5] X. Li, D. Song, P. Zhang, Y. Zhang, Y. Hou, B. Hu, Exploring EEG features in cross-subject emotion recognition, *Front. Neurosci.* 12 (2018) 162.
- [6] X. Mao, Z. Li, Implementing emotion-based user-aware e-learning, in: CHI’09 Ext. Abstr. Hum. Factors Comput. Syst., 2009: pp. 3787–3792.
- [7] G. Chanel, C. Rebetez, M. Bétrancourt, T. Pun, Emotion assessment from physiological signals for adaptation of game difficulty, *IEEE Trans. Syst. Man, Cybern. A Syst. Humans.* 41 (6) (2011) 1052–1063.
- [8] W. Tao, C. Li, R. Song, J. Cheng, Y. Liu, F. Wan, X. Chen, EEG-based emotion recognition via channel-wise attention and self attention, *IEEE Trans. Affect. Comput.*, 2020.
- [9] H. Cui, A. Liu, X. Zhang, X. Chen, K. Wang, X. Chen, EEG-based emotion recognition using an end-to-end regional-asymmetric convolutional neural network, *Knowledge-Based Syst.* 205 (2020), 106243.
- [10] Rab Nawaz, Kit Hwa Cheah, Humaira Nisar, Vooi Voon Yap, Comparison of different feature extraction methods for EEG-based emotion recognition, *Biocybern. Biomed. Eng.* 40 (3) (2020) 910–926.

- [11] Y. Liu, Y. Ding, C. Li, J. Cheng, R. Song, F. Wan, X. Chen, Multi-channel EEG-based emotion recognition via a multi-level features guided capsule network, *Comput. Biol. Med.* 123 (2020), 103927.
- [12] Lawrence M. Ward, Synchronous neural oscillations and cognitive processes, *Trends Cogn. Sci.* 7 (12) (2003) 553–559.
- [13] James A. Coan, John J.B. Allen, Frontal EEG asymmetry as a moderator and mediator of emotion, *Biol. Psychol.* 67 (1-2) (2004) 7–50.
- [14] C. Wei, L. Chen, Z. Song, X. Lou, D. Li, EEG-based emotion recognition using simple recurrent units network and ensemble learning, *Biomed. Signal Process. Control.* 58 (2020), 101756.
- [15] Y.-P. Lin, C.-H. Wang, T.-P. Jung, T.-L. Wu, S.-K. Jeng, J.-R. Duann, J.-H. Chen, EEG-based emotion recognition in music listening, *IEEE Trans. Biomed. Eng.* 57 (2010) 1798–1806.
- [16] A.T. Sohaib, S. Qureshi, J. Hagelbäck, O. Hilborn, P. Jerčić, Evaluating classifiers for emotion recognition using EEG, *Int. Conf. Augment. Cogn.*, Springer (2013) 492–501.
- [17] Wei-Long Zheng, Jia-Yi Zhu, Bao-Liang Lu, Identifying stable patterns over time for emotion recognition from EEG, *IEEE Trans. Affect. Comput.* 10 (3) (2019) 417–429.
- [18] D. Huang, S. Chen, C. Liu, L. Zheng, Z. Tian, D. Jiang, Differences first in asymmetric brain: A bi-hemisphere discrepancy convolutional neural network for EEG emotion recognition, *Neurocomputing* 448 (2021) 140–151.
- [19] X. Wang, T. Zhang, X. Xu, L. Chen, X. Xing, C.L.P. Chen, EEG emotion recognition using dynamical graph convolutional neural networks and broad learning system, in: 2018 IEEE Int. Conf. Bioinforma. Biomed., IEEE, 2018: pp. 1240–1244.
- [20] Peiyang Li, Huan Liu, Yajing Si, Cunbo Li, Fali Li, Xuyang Zhu, Xiaoye Huang, Ying Zeng, Dezhong Yao, Yangsong Zhang, Peng Xu, EEG based emotion recognition by combining functional connectivity network and local activations, *IEEE Trans. Biomed. Eng.* 66 (10) (2019) 2869–2881.
- [21] N. Salankar, P. Mishra, L. Garg, Emotion recognition from EEG signals using empirical mode decomposition and second-order difference plot, *Biomed. Signal Process. Control.* 65 (2021), 102389.
- [22] M. Soleymani, J. Lichtenauer, T. Pun, M. Pantic, A multimodal database for affect recognition and implicit tagging, *IEEE Trans. Affect. Comput.* 3 (1) (2012) 42–55.
- [23] S. Koelstra, C. Muhl, M. Soleymani, Jong-Seok Lee, A. Yazdani, T. Ebrahimi, T. Pun, A. Nijholt, I. Patras, Deep: A database for emotion analysis using physiological signals, *IEEE Trans. Affect. Comput.* 3 (1) (2012) 18–31.
- [24] Jonathan Freeman, S.E. Avons, Don E. Pearson, Wijnand A. IJsselsteijn, IJsselsteijn, Effects of sensory information and prior experience on direct subjective ratings of presence, *Presence Teleoperators Virtual Environ.* 8 (1) (1999) 1–13.
- [25] Monika Pölonen, Marja Salmimaa, Viljakkaisa Aaltonen, Jukka Häkkinen, Jari Takatalo, Subjective measures of presence and discomfort in viewers of color-separation-based stereoscopic cinema, *J. Soc. Inf. Disp.* 17 (5) (2009) 459, <https://doi.org/10.1889/JSD17.5.459>.
- [26] Wijnand IJsselsteijn, Huub de Ridder, Jonathan Freeman, S.E. Avons, Don Bouwhuis, Effects of stereoscopic presentation, image motion, and screen size on subjective and objective corroborative measures of presence, *Presence Teleoperators Virtual Environ.* 10 (3) (2001) 298–311.
- [27] B. Rooney, E. Hennessy, Actually in the cinema: A field study comparing real 3D and 2D movie patrons' attention, emotion, and film satisfaction, *Media Psychol.* 16 (2013) 441–460.
- [28] Ioannis Kakkos, Georgios N. Dimitrakopoulos, Lingyun Gao, Yuan Zhang, Peng Qi, George K. Matsopoulos, Nitish Thakor, Anastasios Bezerianos, Yu Sun, Mental workload drives different reorganizations of functional cortical connectivity between 2D and 3D simulated flight experiments, *IEEE Trans. Neural Syst. Rehabil. Eng.* 27 (9) (2019) 1704–1713.
- [29] N. Mansouri, M. Maleki, T. Kayikcioglu, An EEG-based stereoscopic research of the PSD differences in pre and post 2D&3D movies watching, *Biomed. Signal Process. Control.* 55 (2020), 101642.
- [30] Minchang Yu, Yingjie Li, Feng Tian, Responses of functional brain networks while watching 2D and 3D videos: An EEG study, *Biomed. Signal Process. Control.* 68 (2021) 102613, <https://doi.org/10.1016/j.bspc.2021.102613>.
- [31] J. Marín-Morales, C. Llinás, J. Guixeres, M. Alcañiz, Emotion recognition in immersive virtual reality: From statistics to affective computing, *Sensors (Switzerland)* 20 (2020) 1–26.
- [32] R. Srinivasan, D.M. Tucker, M. Murias, Estimating the spatial Nyquist of the human EEG, *Behav. Res. Methods, Instruments, Comput.* 30 (1998) 8–19.
- [33] J. Song, C. Davey, C. Poulsen, P. Luu, S. Turovets, E. Anderson, K. Li, D. Tucker, EEG source localization: Sensor density and head surface coverage, *J. Neurosci. Methods.* 256 (2015) 9–21.
- [34] A. Al-Nafjan, M. Hosny, Y. Al-Ohabli, A. Al-Wabil, Review and classification of emotion recognition based on EEG brain-computer interface system research: a systematic review, *Appl. Sci.* 7 (2017) 1239.
- [35] Eleni Kroupi, Jean-Marie Vesin, Touradj Ebrahimi, Subject-independent odor pleasantness classification using brain and peripheral signals, *IEEE Trans. Affect. Comput.* 7 (4) (2016) 422–434.
- [36] J. Zhang, M. Chen, S. Zhao, S. Hu, Z. Shi, Y. Cao, ReliefF-based EEG sensor selection methods for emotion recognition, *Sensors.* 16 (2016) 1558.
- [37] Z. Li, X. Tian, L. Shu, X. Xu, B. Hu, Emotion recognition from eeg using rasm and lsm, in: *Int. Conf. Internet Multimed. Comput. Serv.*, Springer, 2017: pp. 310–318.
- [38] M. Chen, J. Han, L. Guo, J. Wang, I. Patras, Identifying valence and arousal levels via connectivity between EEG channels, in: 2015 Int. Conf. Affect. Comput. Intell. Interact., IEEE, 2015: pp. 63–69.
- [39] O. Sporns, The human connectome: a complex network, *Ann. N. Y. Acad. Sci.* 1224 (2011) 109–125.
- [40] I.B. Mauss, M.D. Robinson, Measures of emotion: A review, *Psychology Press*, 2010.
- [41] You-Yun Lee, Shulan Hsieh, Jean Daunizeau, Classifying different emotional states by means of EEG-based functional connectivity patterns, *PLoS ONE* 9 (4) (2014) e95415.
- [42] S. Alhagry, A.A. Fahmy, R.A. El-Khoribi, Emotion recognition based on EEG using LSTM recurrent neural network, *Emotion* 8 (2017) 355–358.
- [43] James A. Russell, A circumplex model of affect, *J. Pers. Soc. Psychol.* 39 (6) (1980) 1161–1178.
- [44] V. Jurcak, D. Tsuzuki, I. Dan, 10/20, 10/10, and 10/5 systems revisited: their validity as relative head-surface-based positioning systems, *Neuroimage*. 34 (2007) 1600–1611.
- [45] A. Delorme, S. Makeig, EEGLAB: An open source toolbox for analysis of single-trial EEG dynamics including independent component analysis, *J. Neurosci. Methods.* 134 (2004) 9–21.
- [46] J. Poza, C. Gómez, M.T. Gutiérrez, N. Mendoza, R. Hornero, Effects of a multi-sensory environment on brain-injured patients: Assessment of spectral patterns, *Med. Eng. Phys.* 35 (2013) 365–375.
- [47] R. Yuvaraj, M. Murugappan, Norlinah Mohamed Ibrahim, Kenneth Sundaraj, Mohd Iqbal Omar, Khairiyah Mohamad, R. Palaniappan, Optimal set of EEG features for emotional state classification and trajectory visualization in Parkinson's disease, *Int. J. Psychophysiol.* 94 (3) (2014) 482–495.
- [48] A. Shakeel, T. Tanaka, K. Kitajo, Time-series prediction of the oscillatory phase of EEG signals using the least mean square algorithm-based AR model, *Appl. Sci.* 10 (2020) 3616.
- [49] S. Hatamikia, A.M. Nasrabadi, N. Shourie, Analysis of inter-hemispheric and intra-hemispheric differences of the correlation dimension in the emotional states based on EEG signals, in: 2015 22nd Iran. Conf. Biomed. Eng., IEEE, 2015: pp. 6–9.
- [50] G. Zhao, Y. Zhang, Y. Ge, Frontal EEG asymmetry and middle line power difference in discrete emotions, *Front. Behav. Neurosci.* 12 (2018) 225.
- [51] James A. Coan, John J.B. Allen, Eddie Harmon-Jones, Voluntary facial expression and hemispheric asymmetry over the frontal cortex, *Psychophysiology* 38 (6) (2001) 912–925.
- [52] Andreas K. Engel, Pascal Fries, Peter König, Michael Brecht, Wolf Singer, Temporal binding, binocular rivalry, and consciousness, *Conscious. Cogn.* 8 (2) (1999) 128–151.
- [53] E. Lowet, M.J. Roberts, P. Bonizzi, J. Karel, P. De Weerd, Quantifying neural oscillatory synchronization: A comparison between spectral coherence and phase-locking value approaches, *PLoS ONE* 11 (2016), e0146443.
- [54] P. Fries, A mechanism for cognitive dynamics: neuronal communication through neuronal coherence, *Trends Cogn. Sci.* 9 (2005) 474–480.
- [55] Yasar Dasdemir, Esen Yıldırım, Serdar Yıldırım, Analysis of functional brain connections for positive-negative emotions using phase locking value, *Cogn. Neurodyn.* 11 (6) (2017) 487–500.
- [56] B.T. Schmidt, A.S. Ghuman, T.J. Huppert, Whole brain functional connectivity using phase locking measures of resting state magnetoencephalography, *Front. Neurosci.* 8 (2014) 141.
- [57] P. Virtanen, R. Gommers, T.E. Oliphant, M. Haberland, T. Reddy, D. Cournapeau, E. Burovski, P. Peterson, W. Weckesser, J. Bright, SciPy 1.0: fundamental algorithms for scientific computing in Python, *Nat. Methods.* 17 (2020) 261–272.
- [58] Huangeng Luo, Xingjie Fang, Bugra Ertas, Hilbert transform and its engineering applications, *AIAA J.* 47 (4) (2009) 923–932.
- [59] Haifao Yu, Xiang Li, Xinyi Lei, Jiang Wang, Modulation effect of acupuncture on functional brain networks and classification of its manipulation with EEG signals, *IEEE Trans. Neural Syst. Rehabil. Eng.* 27 (10) (2019) 1973–1984.
- [60] P. Tewarie, E. van Dellen, A. Hillebrand, C.J. Stam, The minimum spanning tree: an unbiased method for brain network analysis, *Neuroimage*. 104 (2015) 177–188.
- [61] X. Cui, J. Xiao, H. Guo, B. Wang, D. Li, Y. Niu, J. Xiang, J. Chen, Clustering of brain function network based on attribute and structural information and its application in brain diseases, *Front. Neuroinform.* 13 (2020) 79.
- [62] A. Hagberg, P. Swart, D. S. Chult, Exploring network structure, dynamics, and function using NetworkX, Los Alamos National Lab.(LANL), Los Alamos, NM (United States), 2008.
- [63] Ulrik Brandes, On variants of shortest-path betweenness centrality and their generic computation, *Soc. Networks*. 30 (2) (2008) 136–145.
- [64] X. Ma, G. Jiang, S. Fu, J. Fang, Y. Wu, M. Liu, G. Xu, T. Wang, Enhanced network efficiency of functional brain networks in primary insomnia patients, *Front. Psychiatry*. 9 (2018) 46.
- [65] F. Pedregosa, G. Varoquaux, A. Gramfort, V. Michel, B. Thirion, O. Grisel, M. Blondel, P. Prettenhofer, R. Weiss, V. Dubourg, Scikit-learn: Machine learning in Python, *J. Mach. Learn. Res.* 12 (2011) 2825–2830.
- [66] P. Bilgin, K. Agres, N. Robinson, A.A.P. Wai, C. Guan, A comparative study of mental states in 2D and 3D virtual environments using EEG, in: 2019 IEEE Int. Conf. Syst. Man Cybern., IEEE, 2019: pp. 2833–2838.
- [67] L.I.A. U, N. V. Lotova, V.I. Koshkarov, P. Victor, Y.N. Mordvintsev, S.A. Popov, Non-linear dynamic complexity of the human EEG during evoked emotions, (1998).
- [68] L.-W. Ko, O. Komarov, W.D. Hairston, T.-P. Jung, C.-T. Lin, Sustained attention in real classroom settings: An EEG study, *Front. Hum. Neurosci.* 11 (2017) 388.
- [69] Arielle S. Keller, Lisa Payne, Robert Sekuler, Characterizing the roles of alpha and theta oscillations in multisensory attention, *Neuropsychologia*. 99 (2017) 48–63.
- [70] G. Peeters, J. Czapinski, Positive-negative asymmetry in evaluations: The distinction between affective and informational negativity effects, *Eur. Rev. Soc. Psychol.* 1 (1990) 33–60.
- [71] A. Vaish, T. Grossmann, A. Woodward, Not all emotions are created equal: the negativity bias in social-emotional development, *Psychol. Bull.* 134 (2008) 383.

- [72] D.J. Oathes, W.J. Ray, A.S. Yamasaki, T.D. Borkovec, L.G. Castonguay, M. G. Newman, J. Nitschke, Worry, generalized anxiety disorder, and emotion: Evidence from the EEG gamma band, *Biol. Psychol.* 79 (2008) 165–170.
- [73] Dawn R. Collins, J. Guillaume Pelleter, Denis Paré, Slow and fast (gamma) neuronal oscillations in the perirhinal cortex and lateral amygdala, *J. Neurophysiol.* 85 (4) (2001) 1661–1672.
- [74] S.P. Fitzgibbon, K.J. Pope, L. Mackenzie, C.R. Clark, J.O. Willoughby, Cognitive tasks augment gamma EEG power, *Clin. Neurophysiol.* 115 (8) (2004) 1802–1809.
- [75] C. Tallon-Baudry, The roles of gamma-band oscillatory synchrony in human visual cognition, *Front Biosci.* 14 (2009) 26.
- [76] L. Zhu, C. Su, J. Zhang, G. Cui, A. Cichocki, C. Zhou, J. Li, EEG-based approach for recognizing human social emotion perception, *Adv. Eng. Informatics.* 46 (2020), 101191.
- [77] A.S. Heberlein, A.A. Padon, S.J. Gillihan, M.J. Farah, L.K. Fellows, Ventromedial frontal lobe plays a critical role in facial emotion recognition, *J. Cogn. Neurosci.* 20 (2008) 721–733.
- [78] W.-L. Zheng, B.-L. Lu, Investigating critical frequency bands and channels for EEG-based emotion recognition with deep neural networks, *IEEE Trans. Auton. Ment. Dev.* 7 (2015) 162–175.
- [79] S. Wu, X. Xu, L. Shu, B. Hu, Estimation of valence of emotion using two frontal EEG channels, in: 2017 IEEE Int. Conf. Bioinforma. Biomed., IEEE, 2017: pp. 1127–1130.
- [80] R. Carter, The visual cortex, in: *Hum. Brain B. An Illus. Guid. to Its Struct. Funct. Disord.*, Penguin, 2019: pp. 82–87.
- [81] A. Floriano, P.F. Diez, T. Freire Bastos-Filho, Evaluating the influence of chromatic and luminance stimuli on SSVEPs from behind-the-ears and occipital areas, *Sensors.* 18 (2018) 615.
- [82] Y. Qi, Random forest for bioinformatics, in: *Ensemble Mach. Learn.*, Springer, 2012: pp. 307–323.
- [83] D.M. Reif, A.A. Motsinger, B.A. McKinney, J.E. Crowe, J.H. Moore, Feature selection using a random forests classifier for the integrated analysis of multiple data types, in: 2006 IEEE Symp. Comput. Intell. Bioinforma. Comput. Biol., IEEE, 2006: pp. 1–8.
- [84] Emma V.A. Sylvester, Paul Bentzen, Ian R. Bradbury, Marie Clément, Jon Pearce, John Horne, Robert G. Beiko, Applications of random forest feature selection for fine-scale genetic population assignment, *Evol. Appl.* 11 (2) (2018) 153–165.
- [85] M. Huljanah, Z. Rustam, S. Utama, T. Siswantining, Feature selection using random forest classifier for predicting prostate cancer, in: IOP Conf. Ser. Mater. Sci. Eng., IOP Publishing, 2019: p. 52031.
- [86] Ahmet Alkan, M. Kemal Kiyimik, Comparison of AR and Welch methods in epileptic seizure detection, *J. Med. Syst.* 30 (6) (2006) 413–419.